Original Article

Intratumoral and peritumoral radiomics combined with computed tomography features for predicting the invasiveness of lung adenocarcinoma presenting as a subpleural ground-glass nodule with a consolidation-to-tumor ratio ≤50%

Yun Wang[1#], Deng Lyu[1#], Dan Yu[2#], Su Hu[3], Yanqing Ma[4], Wenjun Huang[5], Shaofeng Duan[6], Taohu Zhou[1^], Wenting Tu[1^], Xiuxiu Zhou[1^], Yi Xiao[1^], Li Fan[1^], Shiyuan Liu[1^]

[1]Department of Radiology, Second Affiliated Hospital of Navy Medical University, Shanghai, China; [2]Department of Radiology, Hangzhou Lin'an District First People's Hospital, Hangzhou, China; [3]Department of Radiology, The First Affiliated Hospital of Soochow University, Suzhou, China; [4]Department of Radiology, Zhejiang Provincial People's Hospital, Affiliated People's Hospital of Hangzhou Medical College, Hangzhou, China; [5]Department of Radiology, The Second People's Hospital of Deyang, Deyang, China; [6]GE Healthcare, Precision Health Institution, Shanghai, China

Contributions: (I) Conception and design: Y Wang, L Deng, Y Dan; (II) Administrative support: Y Xiao, L Fan, S Liu; (III) Provision of study materials or patients: S Hu, Y Ma, W Huang; (IV) Collection and assembly of data: L Deng, W Tu, X Zhou; (V) Data analysis and interpretation: S Duan, T Zhou; (VI) Manuscript writing: All authors; (VII) Final approval of manuscript: All authors.

[#]These authors contributed equally to this work.

Correspondence to: Li Fan, MD; Shiyuan Liu, MD. Department of Radiology, Second Affiliated Hospital of Navy Medical University, 415 Fengyang Road, Huangpu District, Shanghai 200003, China. Email: fanli0930@163.com; radiology_cz@163.com.

Background: Preoperative accurate judgment of the degree of invasiveness in subpleural ground-glass lung adenocarcinoma (LUAD) with a consolidation-to-tumor ratio (CTR) ≤50% is very important for the choice of surgical timing and planning. This study aims to investigate the performance of intratumoral and peritumoral radiomics combined with computed tomography (CT) features for predicting the invasiveness of LUAD presenting as a subpleural ground-glass nodule (GGN) with a CTR ≤50%.

Methods: A total of 247 patients with LUAD from our hospital were randomly divided into two groups, i.e., the training cohort (n=173) and the internal validation cohort (n=74) (7:3 ratio). Furthermore, 47 patients from three other hospitals were collected as the external validation cohort. In the training cohort, the differences in clinical-radiological features were compared using univariate and multivariate analyses. The gross tumor volume (GTV) and gross peritumoral tumor volume (GPTV5, GPTV10, and GPTV15) radiomics models were constructed based on intratumoral and peritumoral (5, 10, and 15 mm) radiomics features. Additionally, the radscore of the best radiomics model and clinical risk factors were used to construct a combined model and the predictive efficacy of the model was evaluated in the validation cohorts. Finally, the receiver operating characteristics (ROC) curve and area under the curve (AUC) value were used to evaluate the discriminative ability of the model.

Results: Tumor size and CTR were independent risk factors for predicting the invasiveness of LUAD. The GPTV10 model outperformed the other radiomics models, with AUC values of 0.910, 0.870, and 0.887 in the three cohorts. The AUC values of the combined model were 0.912, 0.874, and 0.892.

Conclusions: A nomogram based on GPTV10-radscore, tumor size, and CTR exhibited high predictive efficiency for predicting the invasiveness of LUAD.

Keywords: Invasiveness; nomogram; radiomics; prediction; lung adenocarcinoma (LUAD)

^ ORCID: Taohu Zhou, 0000-0001-6208-2249; Wenting Tu, 0000-0003-1010-7189; Xiuxiu Zhou, 0000-0003-2405-0566; Yi Xiao, 0000-0002-3212-2892; Li Fan, 0000-0003-4722-3933; Shiyuan Liu, 0000-0003-3420-0310.

Submitted Feb 14, 2024. Accepted for publication Jun 28, 2024. Published online Aug 28, 2024.
doi: 10.21037/jtd-24-243
View this article at: https://dx.doi.org/10.21037/jtd-24-243

Introduction

With the wide application of conventional computed tomography (CT) and the vigorous development of low-dose CT screening programs for lung cancer, numerous ground-glass nodules (GGNs) have been detected (1,2). GGNs refer to the nodules that increase lung density on continuous thin CT without obscuring the original vessels and bronchus that frame the area (3). GGNs can be divided into pure ground glass nodules (pGGNs) and mixed ground glass nodules (mGGNs) based on the presence or absence of solid components on the mediastinal window of CT (4). The pathological characteristics of GGNs lasting more than three months are mostly precursor glandular lesions or lung adenocarcinoma (LUAD) (5). The linear relationship of its occurrence and development follows three stages: precursor glandular lesions, including atypical adenomatous hyperplasia (AAH) and adenocarcinoma in situ (AIS), followed by minimally invasive adenocarcinoma (MIA) and finally invasive adenocarcinoma (IAC) (6).

Recent studies have showed that, for patients with non-small cell lung cancer (NSCLC) clinically staged as T1aN0 (tumor size, ≤2 cm), sublobar resection and lobectomy were associated with similar survival outcomes (7,8). At 6 months postoperatively, a between-group difference of 2 percentage points was measured in the median percentage of predicted forced expiratory volume in 1 second, favoring the sublobar-resection group (8). The domestic consensus on the management of GGNs suspected as LUAD suggests that the appropriate surgical strategy should be selected according to the pathological subtype of lung cancer predicted by imaging, including wedge resection, segmentectomy or lobectomy (9).

Several previous studies have shown that GGNs with a consolidation-to-tumor ratio (CTR) of >50% and the presence of pleural indentation sign are important CT features for predicting the invasiveness of GGN-type LUAD (10-13). For pGGNs and mGGNs with CTR ≤50%, the pathological types are mostly AAH, AIS, and MIA, the growth rate is slow, and the prognosis is excellent. The current study referred to such lesions as "low-risk GGNs". However, IAC also accounts for a considerable proportion of these "low-risk GGNs" especially those in contact with the pleura (12-14). Due to the concern that it is more likely to invade the visceral pleura during the growth process and cause poor prognosis compared to non-touching-pleura GGNs, which may trigger more intensive surveillance and more active treatment. Therefore, accurate identification of MIA and IAC from the "low-risk GGNs" in contact with the pleura is very important for the choice of surgical timing and planning.

Zhao *et al.* (13) explored the risk factors related to the invasiveness of LUAD presenting as pGGN in contact with the pleura on CT, the result showed that the sensitivity and specificity of tumor relative density in differential diagnosis of IAC were 72.3% and 64.7%, respectively, with a relatively low diagnostic performance. However, Zhao and coworkers only evaluated the risk factors and did not build and validate the prediction model. Radiomics can extract multi-dimensional features that cannot be recognized by naked eyes, which can not only maximize the use of image information but also avoid the subjective differences of traditional CT feature evaluation. Jiang *et al.* (14) explored the ability of intratumoral radiomics features to differentiate IAC from MIA. They found that the AUC values were

Highlight box

Key findings

- Tumor size and consolidation-to-tumor ratio (CTR) were independent risk factors for predicting the invasiveness of lung adenocarcinoma (LUAD).
- Compared with the other radiomics models, the GPTV10 radiomics model had the best performance.

What is known and what is new?

- The combined model based on GPTV10 radiomics features, tumor size and CTR exhibited good performance in predicting the invasiveness of LUAD presenting as a subpleural ground-glass nodule (GGN) with a CTR ≤50% before surgery; it provides valuable information for selecting an appropriate diagnosis and treatment plan.

What is the implication, and what should change now?

- This combined model can effectively improve the prediction efficiency of accurately judging the degree of invasiveness of "low-risk GGNs" with pleural contact before surgery and provides valuable information for the formulation of a follow-up plan and the selection of the operation time.

0.892 and 0.862 for the training and validation cohorts, respectively. However, their study only analyzed the predictive efficacy of the intratumoral radiomics model but did not further explore the predictive value of peritumoral radiomics or externally validate their findings, and thus the repeatability and reproducibility of the predictive model were not verified.

Herein, the intratumoral region of "low-risk GGNs" was expanded externally by 5, 10, and 15 mm respectively to obtain the intratumoral and peritumoral fusion region, which was used as a whole volume of interest (VOI) for feature extraction and modeling and was verified in independent internal and external validation cohorts. Compared with the intratumoral radiomics model, the prediction value of the intratumoral and peritumoral radiomics model for predicting the degree of invasiveness of "low-risk GGNs" in contact with the pleura was evaluated, and a combined model was constructed in combination with CT features to explore whether its diagnostic efficiency could be further improved. We present this article in accordance with the TRIPOD reporting checklist (available at https://jtd.amegroups.com/article/view/10.21037/jtd-24-243/rc).

Methods

Patients

The clinico-radiologic data of patients with peripheral LUAD confirmed by pathology after chest CT examination in four hospitals from July 2014 to December 2021 were retrospectively analyzed. The inclusion criteria were as follows: (I) clinical stage IA LUAD (cT1N0M0, i.e., maximum tumor diameter ≤3 cm); (II) pathological diagnosis of MIA or IAC; (III) CT showed pGGNs or mGGNs, 0%≤ CTR ≤50%; (IV) preoperative CT showed that the tumor was subpleural and in contact with the pleura; (V) thin-layer chest CT data within 2 weeks before surgery (layer thickness ≤1 mm). The detailed patient inclusion procedure is shown in *Figure 1*.

The study was conducted in accordance with the Declaration of Helsinki (as revised in 2013). The study was approved by the institutional review board of the Second Affiliated Hospital of Navy Medical University (No. CZ-20210528-01) and individual consent for this retrospective analysis was waived.

Equipment and parameters

Patients in the internal cohort underwent preoperative chest CT examinations with four types of CT machines from three vendors, including the Toshiba Aquilion16 row, GE Light Speed VCT 64 row, Philips Ingenuity 64 row, and Brilliance iCT 128 row CT machines. In the external cohort, the 19 patients from hospital one were scanned with Toshiba Aquilion 16 row, GE Revolution 256 row, GE Discovery 750HD 64 row, Siemens SOMATOM Sensation 64 row and Definition Flash dual-source CT, Dutch Philips Brilliance 16 row and iCT 128 row, and Dutch Philips IQon Spectral CT machines. SOMATOM Definition AS and AS+ 64 row and Philips Brilliance 16 row CT machines were used to scan the 14 patients from Hospital two, whereas GE Discovery 750HD and Optima CT670 64 row CT machines were used to scan the other 14 patients from Hospital three. The patients were instructed to lie in the supine position during the scan, which covered the entire lung field. The parameters were set as follows: tube voltage was set to 120 kVp, with a tube current of 150-250 mAs or automatic tube current regulation, scanning slice thickness and slice increment were 5 mm, and a reconstruction slice thickness and slice increment were 0.625, 1, and 1.5 mm. The lung algorithm or standard algorithm reconstruction was selected, and non-contrast enhanced images were used for analysis.

Clinicopathological and radiological data collection

Patient data were collected, including gender, age, surgical type, pathological type, and visceral pleural invasion (VPI) status. The DICOM images of patients were imported into software (RadiAnt DICOM Viewer 4.2.1, Medixant, Poland) and analyzed by two independent radiologists with 7 years and 10 years of experience who were blinded to the pathological information. The lung window (width: 1,500 HU, level: −500 HU), mediastinal window (width: 300 HU, level: 50 HU), multiplanar reformation (MPR), and maximal intensity projection (MIP) were used to analyze the lesion. For quantitative measures, the average measurements of two independent radiologists were used as the final data. For qualitative indicators, disagreements were discussed until a consensus was reached.

First, the longest diameter of the whole tumor and the consolidation part were measured at the lung window on

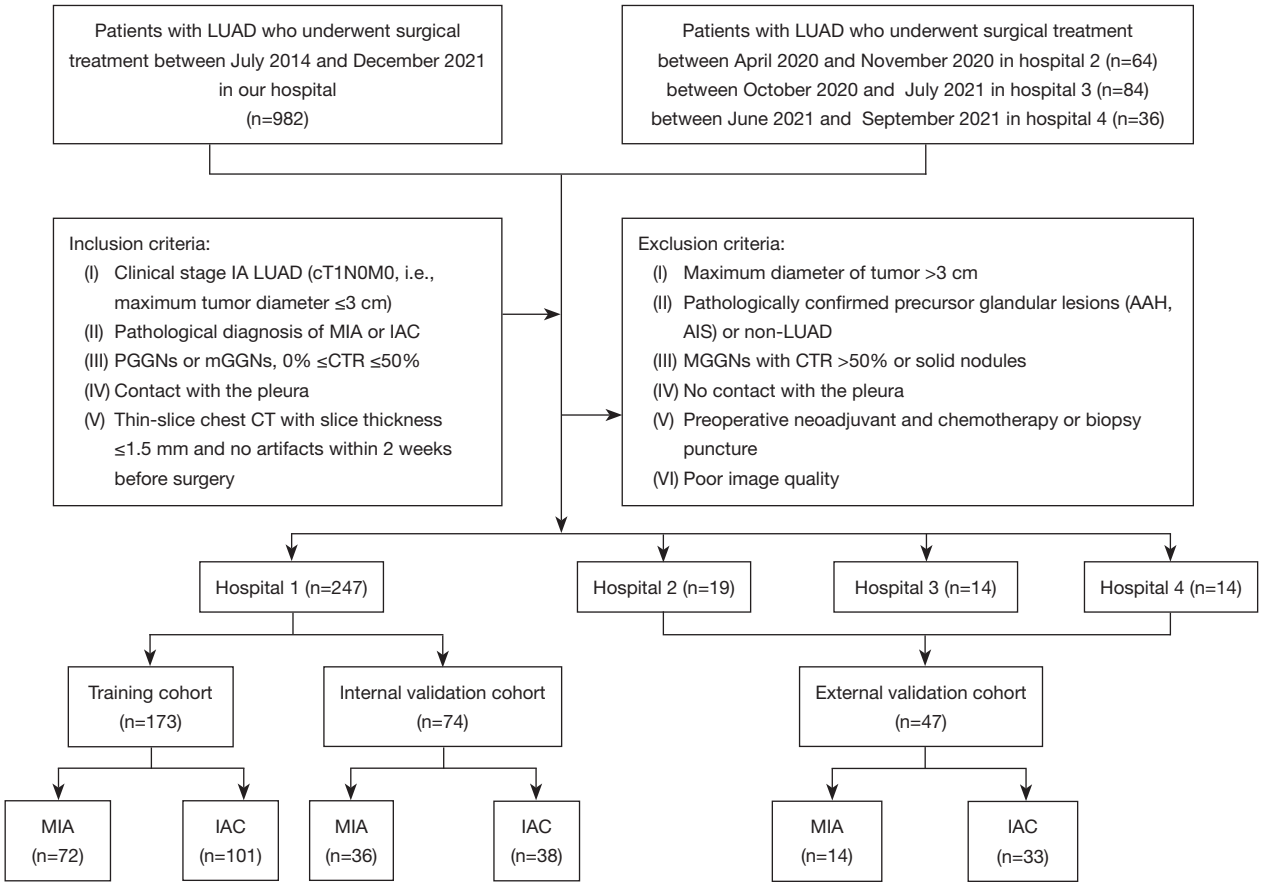

Figure 1 The flow chart for patient selection. Hospital 1, Second Affiliated Hospital of Navy Medical University; Hospital 2, The First Affiliated Hospital of Soochow University; Hospital 3, Zhejiang Provincial People's Hospital, Affiliated People's Hospital of Hangzhou Medical College; Hospital 4, The Second People's Hospital of Deyang. LUAD, lung adenocarcinoma; MIA, minimally invasive adenocarcinoma; IAC, invasive adenocarcinoma; PGGNs, pure ground glass nodules; mGGNs, mixed ground glass nodules; CTR, consolidation-to-tumor ratio; CT, computed tomography; AAH, atypical adenomatous hyperplasia; AIS, adenocarcinoma in situ.

the MPR images, and the CTR was calculated. Second, we assessed the following qualitative CT morphologic features: tumor location, density type (pGGN, mGGN), shape (round, irregular), tumor-lung interface (well-defined, ill-defined), margin (lobulation, spiculation), internal characteristics (vacuole, cavity/cystic airspace), adjacent structure (vascular convergence, pleural indentation, pleural thickening, bronchial change), background of the lobe (normal, emphysema), pleural contact type (indirect contact, direct contact). The definitions of CT features are described in Table S1, Figure S1.

Image segmentation

Standardized image resampling and grayscale discretization were performed on the CT images. ITK-SNAP 3.8.0 software (www.itksnap.org) was used to outline the total volume of the tumor slice by slice along the tumor boundaries, and the gross tumor volume (GTV) was determined, which was used as VOI. GTV was defined as the whole tumor area that was identified within the visible tumor boundary. During segmentation, blood vessels, bronchi, surrounding pleura and atelectatic lung tissue were avoided as much as feasible. Differences in opinion were resolved by discussion and reaching a consensus. Thirty lesions were randomly selected, and two radiologists with 7 years and 10 years of experience who were blinded to the pathological information independently segmented the tumor to evaluate inter-observer repeatability. One month later, the radiologist with 10 years of working experience

performed secondary segmentation on thirty lesions to evaluate intra-observer repeatability. The remaining lesions were segmented by a radiologist with 10 years of working experience. For patients with multiple tumors in the lung, we selected a representative lesion with the largest tumor size for analysis referring to Dercle *et al.* (15). Python 3.1.1 (https://www.python.org) was used to write the expansion algorithm program to capture the range of 5, 10, and 15 mm peritumoral areas based on the segmented GTV to get the VOIs of gross peritumoral tumor volume (GPTV) (labled as GPTV5, GPTV10, and GPTV15, respectively), and pixel filtering was performed on peritumoral non-lung tissues (blood vessels, chest wall, ribs, neck, mediastinum, abdomen) according to the pixel value threshold.

Feature extraction and data preprocessing

The open-source software Pyradiomics (version 3.0.1; https://pyradiomics.readthedocs.io/en/latest/changes.html) was used to extract radiomics features. Overall, 100 original features were extracted, including 14 shape features, 18 first-order statistical features, and 68 texture features [22 gray co-occurrence matrix gray-level co-occurrence matrix (GLCM), 14 gray dependence matrix gray-level dependence matrix (GLDM), 16 gray size area matrix gray-level size zone matrix (GLSZM), and 16 gray run matrix gray-level run length matrix (GLRLM)] (Tables S2, available online: https://cdn.amegroups.cn/static/public/jtd-24-243-1.docx). To obtain high-throughput features, nonlinear intensity transformations (square, square root, logarithmic, and exponential) were applied to image voxels. The Laplacian of Gaussian (LoG) transformation was filtered using sigma values of 1, 2, 3, 4, and 5 mm. Eight wavelet transforms (LLL, LLH, LHL, LHH, HLL, HLH, HHL, and HHH; H stands for a high-pass filter and L for a low-pass filter) were performed for first-order statistical features and texture features, and 1,218 radiomics features were finally obtained (Table S3). Considering that the CT images of the cases included in this study were collected by multiple hospitals and various CT scanners, to reduce the impact of different CT scanners on the images, ComBat (R language SVA package) was used for data preprocessing. Subsequently, the extracted feature values were standardized by Z-score ($Z = x-\mu/\sigma$).

Feature selection and radiomics model construction

Intra-class correlation coefficient (ICC) was used to evaluate the intra-observer and inter-observer consistency of the segmented intratumoral and peritumoral radiomics features, and the "psych" package in R language was used to test the consistency of the radiomics features. Firstly, to mitigate overfitting, the maximal redundancy minimal relevance (mRMR) algorithm and the least absolute shrinkage and selection operator (LASSO) logistic regression method were applied to features with a good consistency (ICC >0.75) in the training cohort to limit the dimension of the features. Secondly, 10-fold cross-validation was used to select the optimal regularization parameter λ value. Under the optimal λ value, features whose coefficients were not equal to 0 were used to construct the radiomics model. Finally, the radscore was calculated based on the linear model by selecting the optimal radiomics features, and the Wilcoxon test was used to compare differences between the MIA group and the IAC group. Overall, GTV, GPTV5, GPTV10, and GPTV15 radiomics models were constructed, and their diagnostic efficiency was evaluated. The model with the highest AUC value in the internal and external validation cohorts was considered the best radiomics model.

Construction of clinical and combined models

The clinico-radiologic features with P<0.1 in the univariate logistic regression analysis were used for multivariate logistic regression analysis, with the criterion of minimization of the Akaike information criterion (16). The clinical model was constructed using the likelihood ratio test to perform backward stepwise feature screening to determine the best combination of risk factors. Next, the radscore of the best radiomics model and clinical risk factors were utilized to construct a combined model and design a nomogram, and its predictive efficacy was evaluated centrally in internal and external validation, as illustrated in *Figure 2*.

Pathological diagnosis

The assessment of VPI status was jointly completed by two experienced pathologists according to the tumor-node-metastasis (TNM) staging standard of lung cancer (8^{th} edition) (17). VPI positive was defined as the tumor invading beyond the elastic fiber layer (PL1) or the tumor invading the visceral pleural surface (PL2). In addition, the growth pattern of tumor cells, the size of invasive components, the presence or absence of vascular invasion, and the spread through air spaces were observed. The pathological grading of the tumors was divided into MIA

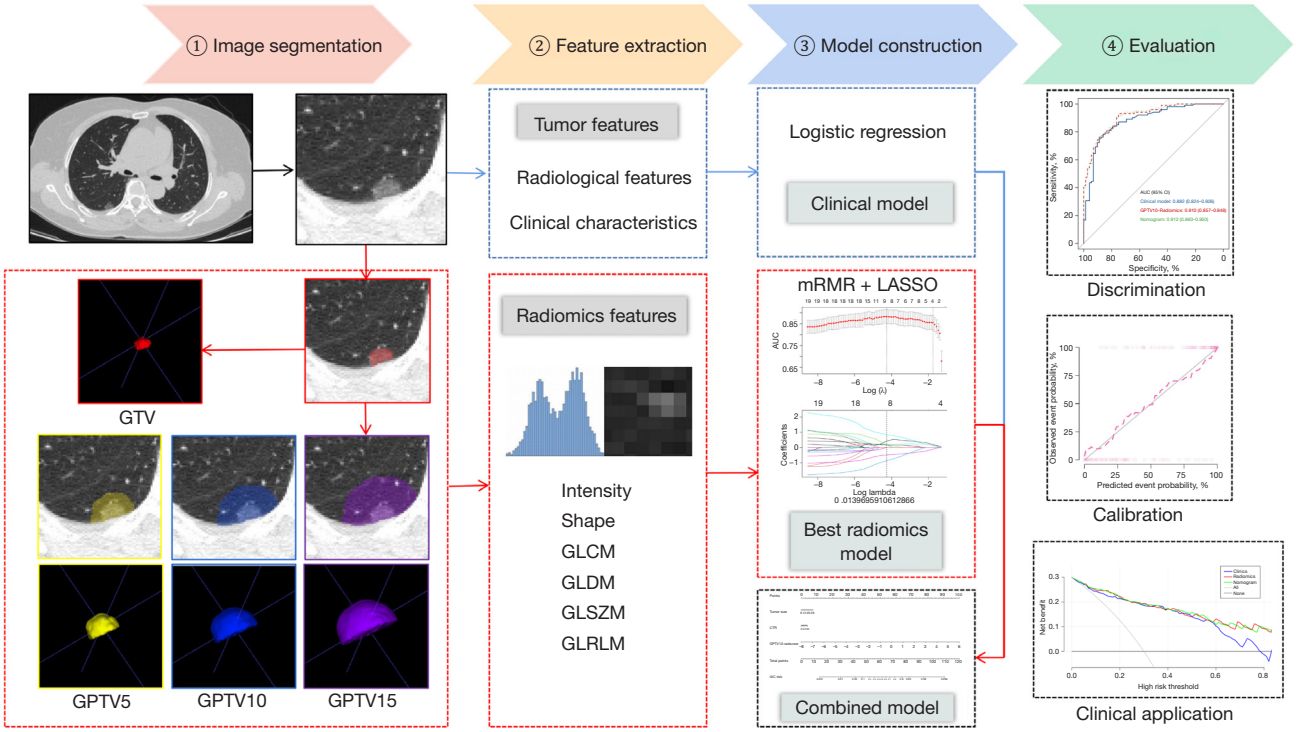

Figure 2 Overall design flow chart of this study. GTV, gross tumor volume; GPTV, gross peritumoral tumor volume.

and IAC. All pathological diagnoses were conducted using pathological reports from our hospital and other hospitals.

Statistical analysis

SPSS 20.0 software and R statistical software (R version 4.2.2) were used for statistical analysis. The Shapiro-Wilk test was used to analyze the normality of measurement data. Measurement data with normal distribution were expressed as mean ± standard deviation ($\bar{x}$±s), and differences between two groups were compared using an independent sample *t*-test. Measurement data with skewed distribution were expressed as median [interquartile range (IQR)], and differences between two groups were compared using a Mann-Whitney *U* test. Categorical data were expressed as the number of cases, and comparison between two groups was performed using Pearson's chi-square test, Yate's correction for continuity, or Fisher's exact test. Regarding the clinical-radiological features screened by univariate and multivariate logistic regression analysis, P<0.05 was considered statistically significant. The receiver operating characteristics curve (ROC) and area under the curve (AUC) value were used to evaluate the diagnostic performance of the model, the Delong test was used to analyze the difference in the AUC value between the models, the Hosmer-Lemeshow test and calibration curve were used to examine the goodness of fit of the model, and decision curve analysis (DCA) was used to assess the clinical applicability of the model. Inter-observer and intra-observer consistency tests were performed using the "psych" package of R language, the "rms" package of R software was employed for multivariate logistic regression analysis and constructing the nomogram and calibration curves, the "pROC" software package was used for ROC curve analysis, and the "rms" package was applied for internal and external validation. The "dca.R" package was used to analyze the decision curve. The kappa coefficient and ICC were used to evaluate the consistency of qualitative and quantitative parameters among observers, respectively.

Results

Patients enrollment

A total of 247 patients with LUAD (247 lesions) from our

Table 1 Clinicopathology characteristics of patients in the training and two validation cohorts

Characteristics	Training cohort (n=173)			Internal validation cohort (n=74)			External validation cohort (n=47)		
	MIA (n=72)	IAC (n=101)	P value	MIA (n=36)	IAC (n=38)	P value	MIA (n=14)	IAC (n=33)	P value
Gender			0.054[a]			0.87[a]			0.12[a]
Female	49 (68.1)	54 (53.5)		24 (66.7)	26 (68.4)		11 (78.6)	18 (54.5)	
Male	23 (31.9)	47 (46.5)		12 (33.3)	12 (31.6)		3 (21.4)	15 (45.5)	
Age (years)	52.8±11.9	58.0±8.2	0.002[d]	49.6±12.3	59.5±12.0	0.001[d]	55.7±14.2	60.4±8.4	0.17[d]
Location			0.80[a]			0.058[a]			0.80[c]
RUL	29 (40.3)	43 (42.6)		6 (16.7)	10 (26.3)		5 (35.8)	16 (48.4)	
RML	4 (5.6)	4 (4.0)		1 (2.8)	6 (15.8)		3 (21.4)	3 (9.1)	
RLL	17 (23.6)	18 (17.8)		6 (16.7)	10 (26.3)		4 (28.6)	9 (27.3)	
LUL	14 (19.4)	26 (25.7)		15 (41.6)	7 (18.4)		1 (7.1)	3 (9.1)	
LLL	8 (11.1)	10 (9.9)		8 (22.2)	5 (13.2)		1 (7.1)	2 (6.1)	
VPI			<0.001[a]			0.14[b]			0.31[b]
Absent	72 (100.0)	81 (80.2)		36 (100.0)	34 (89.5)		14 (100.0)	28 (84.8)	
Present	0 (0.0)	20 (19.8)		0 (0.0)	4 (10.5)		0 (0.0)	5 (15.2)	
Surgery type			<0.001[a]			0.002[a]			<0.001[a]
Sublobectomy	50 (69.4)	32 (31.7)		26 (72.2)	14 (36.8)		11 (78.6)	6 (18.2)	
Lobectomy	22 (30.6)	69 (68.3)		10 (27.8)	24 (63.2)		3 (21.4)	27 (81.8)	

The P value represents the univariate analysis. Data are presented as n (%) or mean ± SD. [a], Pearson's chi-square; [b], Yate's correction for continuity; [c], Fisher's exact test; [d], two independent sample *t*-test. MIA, minimally invasive adenocarcinoma; IAC, invasive adenocarcinoma; RUL, right upper lobe; RML, right middle lobe; RLL, right lower lobe; LUL, left upper lobe; LLL, left lower lobe; VPI, visceral pleural invasion; SD, standard deviation.

hospital were randomly divided into two groups, i.e., the training cohort (n=173) and the internal validation cohort (n=74) (7:3 ratio). Furthermore, 47 patients with LUAD (47 lesions) from three hospitals were used as the external validation cohort, including 19 patients from hospital one, 14 patients from hospital two and 14 patients from hospital three.

Clinicopathological characteristics

Of the 294 patients with LUAD, 122 were MIA group and 172 were IAC group. There was a statistically significant difference in age between the training cohort and the internal validation cohort (P<0.05), and the IAC group was older. VPI positive was only observed in the IAC group but VPI significantly differed between the two groups in the training cohort (P<0.05). VPI negative was more predominant in the MIA group than in the IAC group. There were significant differences in surgery types between the two groups in the three cohorts (P<0.05), and lobectomy was the most common type of surgery in the IAC group (*Table 1*).

Construction and efficacy evaluation of clinical model

For CT features, good consistency between two observers was observed in terms of quantitative parameters (ICC =0.957–0.972), with strong consistency in qualitative indicators (Kappa value =0.830–1.000) (Table S4). In the training cohort, univariate logistic regression analysis results showed that age, density type, tumor size, solid portion size, CTR, bronchial changes, and pleural indentation statistically differed between MIA and IAC groups (P<0.05) (*Table 2*). Due to the collinearity between solid portion size and CTR, only CTR was included in the multivariate logistic regression analysis (Table S5). The results showed that tumor size [odds ratio (OR) =1.23] and CTR (OR =1.06) were independent risk factors for predicting the

Table 2 CT features of tumor in the training and two validation cohorts

Features	Training cohort (n=173)			Internal validation cohort (n=74)			External validation cohort (n=47)		
	MIA (n=72)	IAC (n=101)	P value	MIA (n=36)	IAC (n=38)	P value	MIA (n=14)	IAC (n=33)	P value
Tumor size (mm)	12.2 (9.7, 15.4)	20.6 (16.1, 25.7)	<0.001[e]	11.3 (9.2, 14.1)	18.0 (14.8, 22.1)	<0.001[e]	14.4±5.4	19.1±5.1	0.007[d]
Solid portion size (mm)	0.0 (0.0, 1.7)	6.3 (2.0, 8.8)	<0.001[e]	0.0 (0.0, 2.2)	2.8 (0.0, 8.0)	0.003[e]	3.1±1.8	5.0±3.3	0.02[d]
CTR (%)	0.0 (0.0, 12.4)	31.5 (13.1, 42.0)	<0.001[e]	0.0 (0.0, 14.8)	15.7 (0.0, 38.5)	0.002[e]	27.3 (12.9, 34.4)	27.9 (12.8, 40.1)	0.42[e]
Density type			<0.001[a]			0.009[a]			>0.99[b]
PGGN	51 (70.8)	23 (22.8)		26 (72.2)	16 (42.1)		2 (14.3)	5 (15.2)	
MGGN	21 (29.2)	78 (77.2)		10 (27.8)	22 (57.9)		12 (85.7)	28 (84.8)	
Shape			0.77[a]			0.38[a]			0.88[b]
Irregular	13 (18.1)	20 (19.8)		4 (11.1)	7 (18.4)		2 (14.3)	7 (21.2)	
Round/oval	59 (81.9)	81 (80.2)		32 (88.9)	31 (81.6)		12 (85.7)	26 (78.8)	
Lobulation			0.35[a]			0.49[c]			0.08[c]
Absent	7 (9.7)	6 (5.9)		1 (2.8)	0 (0.0)		2 (14.3)	0 (0.0)	
Present	65 (90.3)	95 (94.1)		35 (97.2)	38 (100.0)		12 (85.7)	33 (100.0)	
Spiculation			0.42[c]			N/A			N/A
Absent	71 (98.6)	101 (100.0)		36 (100.0)	38 (100.0)		14 (100.0)	33 (100.0)	
Present	1 (1.4)	0 (0.0)		0 (0.0)	0 (0.0)		0 (0.0)	0 (0.0)	
Tumor-lung interface			>0.99[c]			>0.99[c]			N/A
Ill-defined	0 (0.0)	1 (1.0)		0 (0.0)	1 (2.6)		0 (0.0)	0 (0.0)	
Well-defined	72 (100.0)	100 (99.0)		36 (100.0)	37 (97.4)		14 (100.0)	33 (100.0)	
Bronchial change			<0.001[a]			0.18[a]			0.13[b]
Absent	67 (93.1)	61 (60.4)		31 (86.1)	28 (73.7)		13 (92.9)	22 (66.7)	
Present	5 (6.9)	40 (39.6)		5 (13.9)	10 (26.3)		1 (7.1)	11 (33.3)	
Vacuole			0.41[a]			0.48[a]			0.35[b]
Absent	56 (77.8)	73 (72.3)		29 (80.6)	28 (73.7)		8 (57.1)	25 (75.8)	
Present	16 (22.2)	28 (27.7)		7 (19.4)	10 (26.3)		6 (42.9)	8 (24.2)	
Cavity/cystic airspace			0.21[a]			>0.99[b]			0.43[b]
Absent	67 (93.1)	88 (87.1)		34 (94.4)	35 (92.1)		14 (100.0)	29 (87.9)	
Present	5 (6.9)	13 (12.9)		2 (5.6)	3 (7.9)		0 (0.0)	4 (12.1)	
Vascular convergence			0.59[b]			N/A			N/A
Absent	71 (98.6)	97 (96.0)		36 (100.0)	38 (100.0)		14 (100.0)	33 (100.0)	
Present	1 (1.4)	4 (4.0)		0 (0.0)	0 (0.0)		0 (0.0)	0 (0.0)	
Emphysema			0.15[b]			0.49[c]			N/A
Absent	72 (100.0)	96 (95.0)		35 (97.2)	38 (100.0)		14 (100.0)	33 (100.0)	
Present	0 (0.0)	5 (5.0)		1 (2.8)	0 (0.0)		0 (0.0)	0 (0.0)	
Pleural indentation			0.04[a]			0.66[a]			0.63[a]
Absent	43 (59.7)	44 (43.6)		17 (47.2)	16 (42.1)		7 (50.0)	19 (57.6)	

Table 2 (*continued*)

Table 2 (*continued*)

Features	Training cohort (n=173)			Internal validation cohort (n=74)			External validation cohort (n=47)		
	MIA (n=72)	IAC (n=101)	P value	MIA (n=36)	IAC (n=38)	P value	MIA (n=14)	IAC (n=33)	P value
Present	29 (40.3)	57 (56.4)		19 (52.8)	22 (57.9)		7 (50.0)	14 (42.4)	
Contact type			0.11[a]			0.02[a]			0.08[a]
Indirect contact	15 (20.8)	32 (31.7)		4 (11.1)	13 (34.2)		3 (21.4)	16 (48.5)	
Direct contact	57 (79.2)	69 (68.3)		32 (88.9)	25 (65.8)		11 (78.6)	17 (51.5)	
Pleural thickening			0.005[a]			0.92[a]			>0.99[b]
Absent	10 (13.9)	33 (32.7)		25 (69.4)	26 (68.4)		12 (85.7)	27 (81.8)	
Present	62 (86.1)	68 (67.3)		11 (30.6)	12 (31.6)		2 (14.3)	6 (18.2)	

The P value represents the univariate analysis. Data are presented as n (%), mean ± SD, or median (IQR). [a], Pearson's chi-square; [b], Yate's correction for continuity; [c], Fisher's exact test; [d], two independent sample *t*-test; [e], Mann-Whitney U test. CT, computed tomography; MIA, minimally invasive adenocarcinoma; IAC, invasive adenocarcinoma; CTR, consolidation-to-tumor ratio; PGGN, pure ground glass nodule; MGGN, mixed ground glass nodule; SD, standard deviation; IQR, interquartile range.

Table 3 Univariate and multivariate logistic regression analysis of factors in the training cohort

Variables	Univariate logistic regression analysis		Multivariate logistic regression analysis	
	OR (95% CI)	P value	OR (95% CI)	P value
Gender	1.85 (0.99–3.49)	0.055		
Age (years)	1.05 (1.02–1.09)	0.001		
Density type	8.24 (4.21–16.74)	<0.001		
Tumor size (mm)	1.31 (1.21–1.42)	<0.001	1.23 (1.13–1.34)	<0.001
Solid portion size (mm)	1.42 (1.28–1.60)	<0.001		
CTR (%)	1.08 (1.06–1.11)	<0.001	1.06 (1.03–1.08)	<0.001
Bronchial change	8.79 (3.26–23.70)	<0.001		
Pleural indentation	1.92 (1.04–3.57)	0.04		

OR, odds ratio; CI, confidence interval; CTR, consolidation-to-tumor ratio.

invasiveness of LUAD (*Table 3*). The AUC values of the clinical model were 0.882, 0.840, and 0.745 in the three cohorts.

Construction and efficacy evaluation of the radiomics model

In total, 1,218 radiomics features were extracted from the VOI of GTV, GPTV5, GPTV10, and GPTV15, respectively. Among them, 73.9% (900/1,218) of GTV features, 91.5% (1,114/1,218) of GPTV5 features, 96.7% (1,178/1,218) of GPTV10 features, and 97.5% (1,187/1,218) of GPTV15 features had good repeatability, the inter-observer and intra-observer ICC values were greater than 0.75. For the features with ICC >0.75, the mRMR algorithm was used to eliminate redundant and irrelevant features, and 30 features were retained in each group. Then LASSO logistic regression algorithm was used to select the optimized feature subset to establish the final model. Next, 10-fold cross-validation was used to select the value of the optimal hyperparameter λ, in which the optimal λ values of GTV, GPTV5, GPTV10, and GPTV15 radiomics models were 0.017, 0.007, 0.014, and 0.020, respectively (Figure S2). Based on the optimal λ value, 12, 11, 8, and 10 features were selected respectively to construct the radiomics models of GTV, GPTV5, GPTV10, and

Table 4 The predictive efficacy of GTV, GPTV5, GPTV10, GPTV15 model in three cohorts

Model	Cohort	AUC (95% CI)	Cut-off	Accuracy (%)	Sensitivity (%)	Specificity (%)
GTV	Training	0.905 (0.851–0.944)	0.311	82.66	84.16	80.56
	Internal validation	0.817 (0.710–0.898)		71.62	65.79	77.78
	External validation	0.855 (0.722–0.941)		78.72	87.88	57.14
GPTV5	Training	0.910 (0.858–0.948)	–0.115	84.39	87.13	80.56
	Internal validation	0.834 (0.730–0.910)		77.03	76.32	77.78
	External validation	0.861 (0.729–0.945)		82.98	84.85	78.57
GPTV10	Training	0.910 (0.857–0.948)	–0.405	85.55	93.07	75.00
	Internal validation	0.870 (0.771–0.937)		79.73	81.58	77.78
	External validation	0.887 (0.761–0.961)		85.11	87.88	78.57
GPTV15	Training	0.889 (0.832–0.931)	–0.096	82.66	86.14	77.78
	Internal validation	0.845 (0.742–0.919)		77.03	71.05	83.33
	External validation	0.870 (0.740–0.950)		82.98	81.82	85.71

GTV, gross tumor volume; GPTV, gross peritumoral tumor volume; AUC, area under the curve; CI, confidence interval.

GPTV15, respectively (Figure S3). The features used for model construction and their ICC details are provided in Table S6. The radscore formulas for the four radiomics models can be found in Table S7. The radscore of the IAC group was higher than that of the MIA group, and the differences were statistically significant (P<0.05) (Figure S4). The group with the highest AUC value in the internal validation and external validation cohorts was selected as the best radiomics model, and the results showed that the GPTV10 radiomics model had the best performance, with AUC values of 0.910, 0.870, and 0.887 in the three cohorts (*Table 4*, Figure S5). The Delong test showed that GPTV10 radiomics models were superior to those of GPTV15 in the training cohort (P=0.01) and those of GTV in the internal validation cohort (P=0.04).

Construction and efficacy evaluation of the combined model

A combined model was constructed and a nomogram was developed based on GPTV10-radscore and clinical risk factors (*Figure 3*). The combined model formula was as follows: Nomoscore = (Intercept) × –0.886 + tumor size × 0.045 + CTR × 0.011 + radscore × 1.041, and its AUC values were 0.912, 0.874, and 0.892 in the three cohorts (*Table 5*). An example of the nomogram in clinical application can be found in Figure S6. ROC curves of the clinical model, GPTV10 radiomics model, and combined model in the three cohorts are presented in *Figure 4*. The Delong test showed that the performance of the combined model was better than that of the clinical model in the training cohort and the external validation cohort (P=0.03 and 0.01, respectively), and the performance of the GPTV10 radiomics model was better than that of the clinical model in the external validation cohort (P=0.02). The Hosmer-Lemeshow test showed that the combined model fitted well in the three cohorts (P=0.32, 0.08, and 0.72, respectively), and the calibration curve showed that the predicted probability value of the combined model was in good agreement with the real situation (*Figure 5*). The DCA curve revealed that the combined model had a better benefit than the clinical model and the GPTV10 radiomics model in predicting the invasiveness of LUAD (*Figure 6*).

Discussion

The study established a combined model based on GPTV10-radscore and CT features, and the AUC of the internal validation and the external validation cohort were 0.874 and 0.892, respectively. This model can effectively improve the prediction efficiency of accurately judging the degree of invasiveness of "low-risk GGNs" with pleural contact before surgery and provide valuable information for the formulation of reasonable follow-up and treatment strategy.

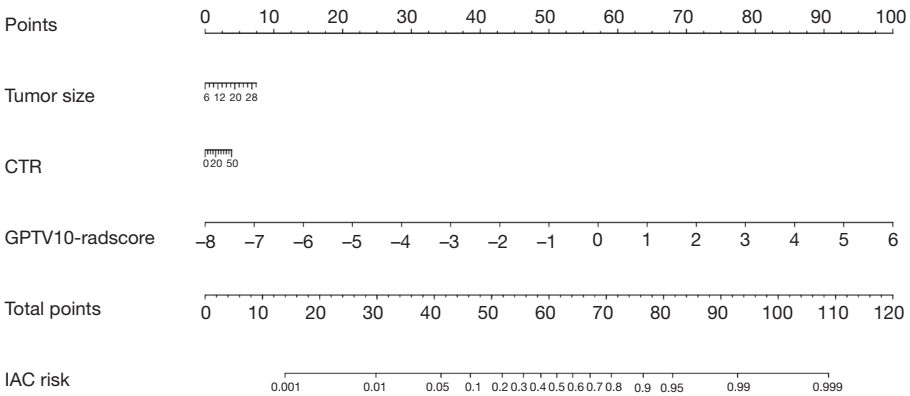

Figure 3 Nomogram for preoperative prediction of the degree of invasiveness based on intratumoral and peritumoral radiomics and CT features in the low-risk GGNs. CT, computed tomography; GGNs, ground glass nodules; CTR, consolidation-to-tumor ratio; IAC, invasive adenocarcinoma; GPTV, gross peritumoral tumor volume.

Table 5 The predictive efficacy of clinical model, GPTV10 model and combined model in three cohorts

Model	Cohort	Cut-off	AUC (95% CI)	Accuracy (%)	Sensitivity (%)	Specificity (%)	PPV (%)	NPV (%)
Clinical	Training	0.634	0.882 (0.824–0.926)	81.50	76.24	88.89	90.59	72.73
	Internal validation		0.840 (0.737–0.915)	67.57	47.37	88.89	81.82	61.54
	External validation		0.745 (0.596–0.860)	63.83	66.67	57.14	78.57	42.11
GPTV10	Training	–0.405	0.910 (0.857–0.948)	85.55	93.07	75.00	83.93	88.52
	Internal validation		0.870 (0.771–0.937)	79.73	81.58	77.78	79.49	80.00
	External validation		0.887 (0.761–0.961)	85.11	87.88	78.57	90.63	73.33
Combined	Training	–0.441	0.912 (0.860–0.950)	84.97	91.09	76.39	84.40	85.94
	Internal validation		0.874 (0.777–0.940)	77.03	78.38	75.68	76.32	77.78
	External validation		0.892 (0.767–0.963)	78.72	42.86	93.94	75.00	79.49

GPTV, gross peritumoral tumor volume; AUC, area under the curve; CI, confidence interval; PPV, positive predictive value; NPV, negative predictive value.

Compared with previous studies (13,14), our study has some innovative points in patient enrollment and research methods. Firstly, according to the latest pathological classification of LUAD released in 2021, AAH and AIS are classified as precursor glandular lesions and are removed from the classification of malignant tumors (6). In other words, GGNs at this stage belong to the category of benign nodules; thus, GGNs with pathologic classification of AAH and AIS were not included as research objects in the present study, which is different from Zhao's study (13). Secondly, our study explored the value of radiomics models based on GTV and GPTV with different peritumoral areas for predicting VPI status, no similar research has been reported before. Thirdly, based on the TRIPOD statement, different prediction models were established, and a multi-center dataset was included for internal and external validation of the model to verify the generalization of the models, which was lacking in previous studies.

In the previous case collection process of this study, it was found that no pathological VPI occurred regardless of the size and shape of the pGGNs, whether the adjacent pleura was indentation or thickened, and if the mediastinal window showed no solid components inside, which is consistent with previous reports (18,19). This finding helps to eliminate preoperative concerns about VPI in pGGN patients with pleural contact, adding evidence for clinical

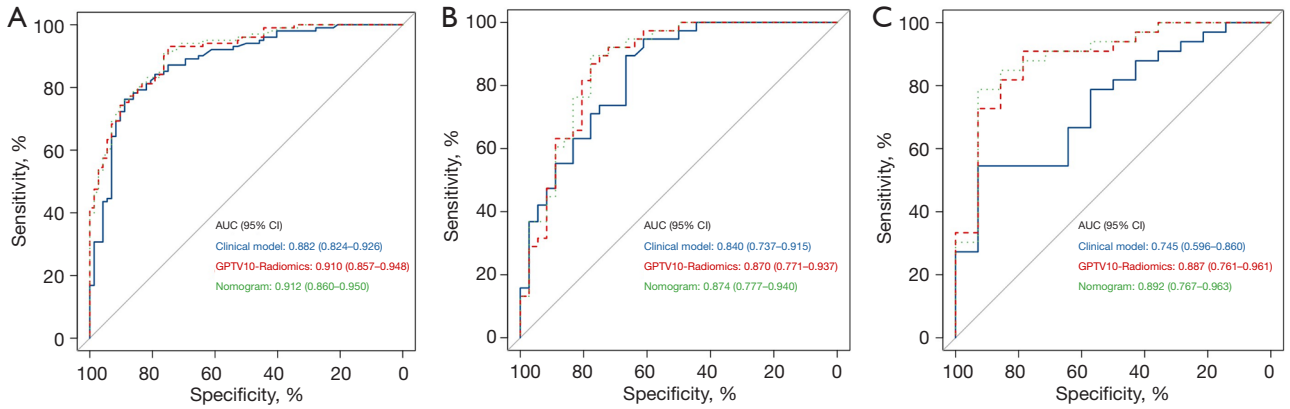

Figure 4 ROC curve analysis of the clinical model, GPTV10 radiomics model, combined model in three cohorts. (A) The training cohort; (B) the internal validation cohort; (C) the external validation cohort. ROC, receiver operating characteristics; GPTV, gross peritumoral tumor volume; AUC, area under the ROC curve; CI, confidence interval.

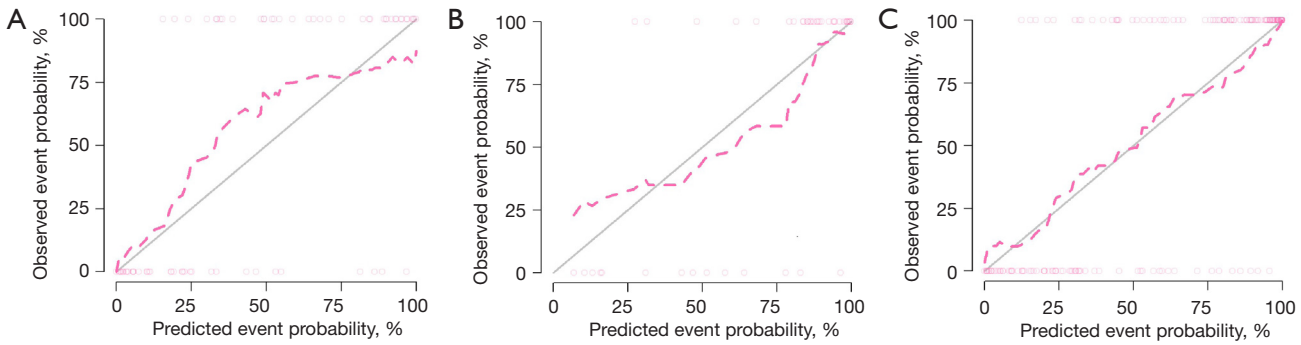

Figure 5 The calibration curves of combined model in the three cohorts. (A) the training cohort; (B) the internal validation cohort; (C) the external validation cohort.

decision-making.

Pathologically, it was found that AAH, AIS, and MIA consist of type II alveolar epithelial cells or Clara cells with the same morphology and anastomosis along the alveolar wall and the respiratory bronchiole wall, with the maximum diameter of the infiltrating lesion ≤5 mm, which do not invade the visceral pleura. On CT, most of these lesions are pGGN or mGGN with less solid components (5,6). Further tumor cell proliferation and accumulation increase cell density, decreased alveolar ventilation, and lead to the occurrence of reactive fibroplasia. The maximum diameter of the infiltrating lesion >5 mm is considered as IAC, and CT shows increased GGN density and increased proportion of solid components (5,6). Therefore, this study found that for GGN with subpleural CTR ≤50%, the proportion of mGGN in the IAC group was higher, the tumor and solid portion sizes were larger, and the CTR was higher, which is consistent with previous reports (20,21). In addition, regarding qualitative indicators, it has been found that the pleural indentation sign and bronchial changes were more common in the IAC group because the intratumoral infiltration was higher in the IAC group than in the MIA group and the degree of reactive fibroplasia was more severe, which invaded and pulled the local bronchial wall and pleura, resulting in morphological changes, corresponding to previous studies (13).

Furthermore, it was found that spiculation and vascular convergence accounted for 0.34% and 1.70% of the total data cohort, respectively. The reason may be that the pathological tumor cells of GGNs with CTR ≤50% were strongly adherent, and the probability of spreading and infiltrating into surrounding tissues was low; hence,

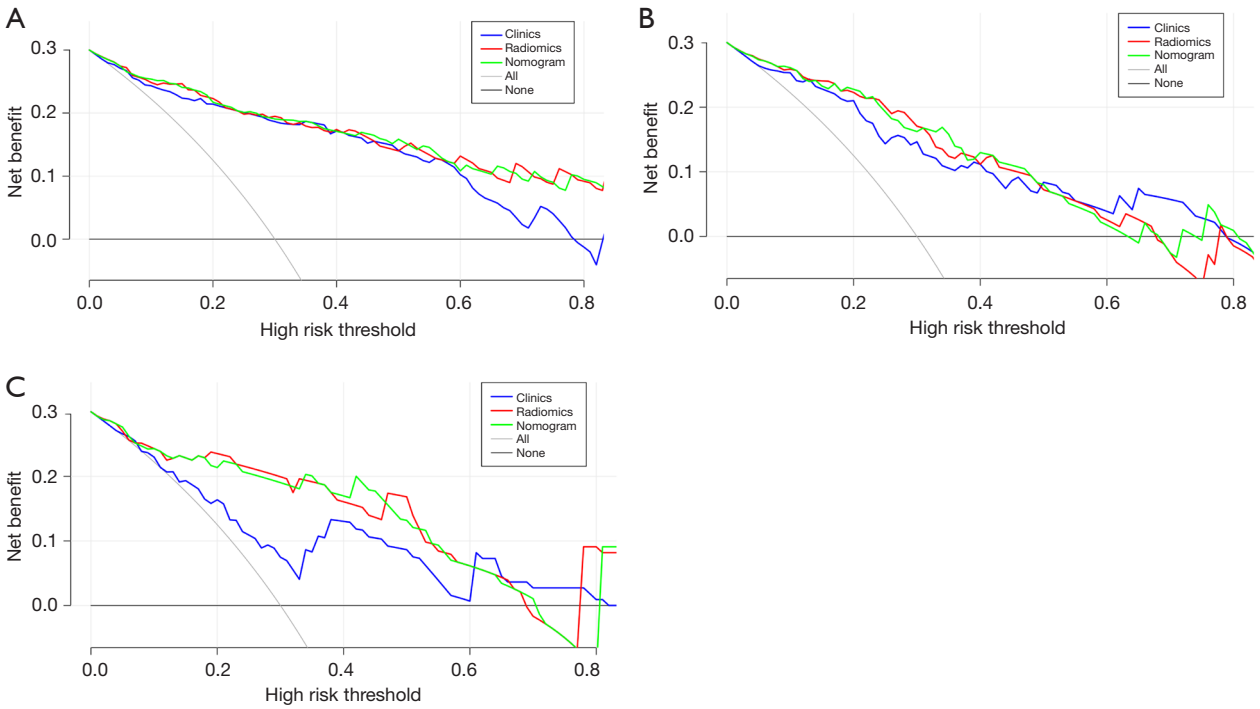

Figure 6 The decision curve shows that the combined model has better clinical application value than the clinical model and GPTV10 radiomics model in the three cohorts. (A) The training cohort; (B) the internal validation cohort; (C) the external validation cohort. GPTV, gross peritumoral tumor volume.

spiculation was rare. Meanwhile, there was less reactive fiber hyperplasia in the tumor, which was insufficient to pull the adjacent vascular bundles to converge to the tumor; therefore, vascular convergence was rare. It was previously reported that solid nodules are more common in lung cancer complicated with emphysema and the pathological grade of the tumor is higher (22). Therefore, the sign complicated with emphysema in this group was also rare, accounting for only 2.04% of the total data cohort.

Multivariate logistic regression analysis showed that only two quantitative variables, tumor size and CTR, were independent risk factors, which may be caused by the large subjectivity in the evaluation of qualitative CT features and the overlap of CT features between IAC and MIA. The diagnostic efficacy of the clinical prediction model built based on these two factors was the highest in the training cohort than in the internal validation and external validation cohorts (AUC =0.882 *vs.* 0.840 and 0.745), and there was an overfitting phenomenon, which may be explained by two reasons. Firstly, the solid portions inside the GGN not only represent the infiltrating part of the tumor but may also be caused by fibroblast proliferation, alveolar collapse, inflammatory cell infiltration, and mucous secreted by the tumor (23). Secondly, a considerable proportion of IAC are pGGNs with no internal solid portions (13,14).

Multiple studies have been conducted to investigate the value of intratumoral and peritumoral radiomics in predicting the degree of invasiveness of subsolid nodules or pGGNs (14,24,25), including the identification of AIS+MIA and IAC (24), MIA and IAC (14,25). Because of the different types and outcome factors in the cases, the radiomics feature extraction method, and the differences in the modeling algorithm, studies on the radiomics feature modeling are endless and similar but have made a more satisfactory prediction (internal validation cohort AUC range of 0.813–0.888). This fully demonstrates that intratumoral heterogeneity and peritumoral microenvironment differences of lung nodules can be quantified by radiomics features, which is also the theoretical basis for further exploration of intratumoral and peritumoral radiomics features to predict the invasiveness of "low-risk GGNS" in contact with the pleura in the current study. Based on the precise tumor segmentation, this study automatically expanded the peritumoral regions with three

different gradient ranges to obtain four radiomics models, namely GTV, GPTV5, GPTV10, and GPTV15, to explore the most efficient radiomics model, and a multicenter study was conducted to evaluate the generalization of the model.

The results showed that GPTV10 radiomics model exhibited the best performance. Based on the VOI of GPTV10, eight best radiomics features were selected, including the Major Axis Length of 1 shape features, the 10 Percentile of 1 first-order features, 6 texture features, namely Zone Entropy, Small Area Low Gray Level Emphasis, Cluster Tendency, Cluster Prominence, Imc2, Correlation. Zone Entropy and Small Area Low Gray Level Emphasis are parameters of GLSZM and principally provide information on the uniform area size of each gray level on the 3D image. Cluster Tendency, Cluster Prominence, Imc2 and Correlation are parameters of GLCM mainly used to evaluate the spatial relationship between pixels and describe the frequency of appearance of specific pixel combinations in the image. These eight radiomics features comprise information related to tumor maximum diameter, CT value, and the distribution of image texture. Some of these radiomics features demonstrate close associations with the semantic features outlined in this study. Together, they provide a comprehensive representation of tumor size, density, and internal heterogeneity, offering insights into the biological behavior of tumors. The AUC of GPTV10 radiomics model in the three cohorts were 0.910, 0.870 and 0.887, respectively. The model was robust and effective, and was superior to previous models for predicting pGGN invasiveness in contact with pleuras based on intratumoral radiomics features (14,25). The model can provide a basis for preoperative non-invasive diagnosis of subpleural GGN invasiveness.

In this study, a combined model was constructed comprising the radscore of GPTV10 radiomics model and clinical risk factors. Results of the Delong test showed that the prediction performance of the combined model was better than that of the clinical model in the training cohort and the external validation cohort ($P<0.05$), and it was attributed to the excellent prediction performance of the GPTV10 radiomics model. The calibration curve analysis revealed that the predicted probability values of the combined model were in good agreement with the real situation in the three cohorts, and the P values of the Hosmer-Lemeshow test were all more than 0.05, indicating that the model had a good goodness of fit. DCA results showed that the combined model achieved good effects relative to the clinical model and the radiomics model.

There are some limitations in this study. Firstly, given that this is a retrospective study, there may be some bias in the selection of samples. Secondly, the external validation cohort had a relatively small sample size, which inevitably led to a degree of overfitting in the model. Thirdly, CT images from multiple hospitals were included, and there were large differences in images due to use of different CT models and scanning protocols. However, we adopted a standard radiomics analysis process and standardized resampling of CT images to minimize the influence of image discrepancies. Fourthly, it is difficult to explain the biological significance of some of the radiomics features, so relevant image-genomics studies can be carried out in the future to improve the biological interpretability of the radiomics model.

Conclusions

In conclusion, our results show that pGGNs do not invade the visceral pleura. The combined model based on GPTV10 radiomics features, tumor size and CTR exhibited good performance in predicting the invasiveness of ground-glass LUAD with subpleural CTR ≤50% before surgery, and it provides valuable information for selecting an appropriate diagnosis and treatment plan.

Acknowledgments

Funding: This research was funded by National Key R&D Program of China (2022YFC2010000, 2022YFC2010002, 2022YFC2010005), Key Program of National Natural Science Foundation of China (81930049), National Natural Science Foundation of China (82171926, 82202140), Shanghai Sailing Program (20YF1449000), Shanghai Science and Technology Innovation Action Plan Program (19411951300), Clinical Innovative Project of Shanghai Changzheng Hospital (2020YLCYJ-Y24), and Program of Science and Technology Commission of Shanghai Municipality (21DZ2202600).

Footnote

Reporting Checklist: The authors have completed the TRIPOD reporting checklist. Available at https://jtd.amegroups.com/article/view/10.21037/jtd-24-243/rc

Data Sharing Statement: Available at https://jtd.amegroups.com/article/view/10.21037/jtd-24-243/dss

Peer Review File: Available at https://jtd.amegroups.com/article/view/10.21037/jtd-24-243/prf

Conflicts of Interest: All authors have completed the ICMJE uniform disclosure form (available at https://jtd.amegroups.com/article/view/10.21037/jtd-24-243/coif). S.D. is an employee of GE Healthcare, Precision Health Institution, Shanghai, China. The other authors have no conflicts of interest to declare.

Ethical Statement: The authors are accountable for all aspects of the work in ensuring that questions related to the accuracy or integrity of any part of the work are appropriately investigated and resolved. The study was conducted in accordance with the Declaration of Helsinki (as revised in 2013). The study was approved by the institutional review board of the Second Affiliated Hospital of Navy Medical University (No. CZ-20210528-01) and individual consent for this retrospective analysis was waived.

References

1. Yip R, Henschke CI, Xu DM, et al. Lung Cancers Manifesting as Part-Solid Nodules in the National Lung Screening Trial. AJR Am J Roentgenol 2017;208:1011-21.
2. Vlahos I, Stefanidis K, Sheard S, et al. Lung cancer screening: nodule identification and characterization. Transl Lung Cancer Res 2018;7:288-303.
3. Kakinuma R, Muramatsu Y, Kusumoto M, et al. Solitary Pure Ground-Glass Nodules 5 mm or Smaller: Frequency of Growth. Radiology 2015;276:873-82.
4. Naidich DP, Bankier AA, MacMahon H, et al. Recommendations for the management of subsolid pulmonary nodules detected at CT: a statement from the Fleischner Society. Radiology 2013;266:304-17.
5. Travis WD, Brambilla E, Nicholson AG, et al. The 2015 World Health Organization Classification of Lung Tumors: Impact of Genetic, Clinical and Radiologic Advances Since the 2004 Classification. J Thorac Oncol 2015;10:1243-60.
6. WHO Classification of Tumours Editorial Board, WHO classification of tumours. Thoracic tumours. 5th ed. Lyon: IARC Press, 2021.
7. Altorki N, Wang X, Damman B, et al. Lobectomy, segmentectomy, or wedge resection for peripheral clinical T1aN0 non-small cell lung cancer: A post hoc analysis of CALGB 140503 (Alliance). J Thorac Cardiovasc Surg 2024;167:338-347.e1.
8. Altorki N, Wang X, Kozono D, et al. Lobar or Sublobar Resection for Peripheral Stage IA Non-Small-Cell Lung Cancer. N Engl J Med 2023;388:489-98.
9. Jiang G, Chen C, Zhu Y, et al. Shanghai Pulmonary Hospital Experts Consensus on the Management of GroundGlass Nodules Suspected as Lung Adenocarcinoma (Version 1). Zhongguo Fei Ai Za Zhi 2018;21:147-59.
10. Suzuki K, Koike T, Asakawa T, et al. A prospective radiological study of thin-section computed tomography to predict pathological noninvasiveness in peripheral clinical IA lung cancer (Japan Clinical Oncology Group 0201). J Thorac Oncol 2011;6:751-6.
11. Asamura H, Hishida T, Suzuki K, et al. Radiographically determined noninvasive adenocarcinoma of the lung: survival outcomes of Japan Clinical Oncology Group 0201. J Thorac Cardiovasc Surg 2013;146:24-30.
12. Meng Y, Liu CL, Cai Q, et al. Contrast analysis of the relationship between the HRCT sign and new pathologic classification in small ground glass nodule-like lung adenocarcinoma. Radiol Med 2019;124:8-13.
13. Zhao Q, Wang JW, Yang L, et al. CT diagnosis of pleural and stromal invasion in malignant subpleural pure ground-glass nodules: an exploratory study. Eur Radiol 2019;29:279-86.
14. Jiang Y, Che S, Ma S, et al. Radiomic signature based on CT imaging to distinguish invasive adenocarcinoma from minimally invasive adenocarcinoma in pure ground-glass nodules with pleural contact. Cancer Imaging 2021;21:1.
15. Dercle L, Fronheiser M, Lu L, et al. Identification of Non-Small Cell Lung Cancer Sensitive to Systemic Cancer Therapies Using Radiomics. Clin Cancer Res 2020;26:2151-62.
16. Portet S. A primer on model selection using the Akaike Information Criterion. Infect Dis Model 2020;5:111-28.
17. Travis WD, Asamura H, Bankier AA, et al. The IASLC Lung Cancer Staging Project: Proposals for Coding T Categories for Subsolid Nodules and Assessment of Tumor Size in Part-Solid Tumors in the Forthcoming Eighth

Edition of the TNM Classification of Lung Cancer. J Thorac Oncol 2016;11:1204-23.
18. Kim HJ, Cho JY, Lee YJ, et al. Clinical Significance of Pleural Attachment and Indentation of Subsolid Nodule Lung Cancer. Cancer Res Treat 2019;51:1540-8.
19. Ahn SY, Park CM, Jeon YK, et al. Predictive CT Features of Visceral Pleural Invasion by T1-Sized Peripheral Pulmonary Adenocarcinomas Manifesting as Subsolid Nodules. AJR Am J Roentgenol 2017;209:561-6.
20. Lee SM, Park CM, Goo JM, et al. Invasive pulmonary adenocarcinomas versus preinvasive lesions appearing as ground-glass nodules: differentiation by using CT features. Radiology 2013;268:265-73.
21. Lee SM, Goo JM, Lee KH, et al. CT findings of minimally invasive adenocarcinoma (MIA) of the lung and comparison of solid portion measurement methods at CT in 52 patients. Eur Radiol 2015;25:2318-25.
22. Lim CG, Shin KM, Lim JK, et al. Emphysema is associated with the aggressiveness of COPD-related adenocarcinomas. Clin Respir J 2020;14:405-12.
23. Park CM, Goo JM, Lee HJ, et al. Nodular ground-glass opacity at thin-section CT: histologic correlation and evaluation of change at follow-up. Radiographics 2007;27:391-408.
24. Wu L, Gao C, Ye J, et al. The value of various peritumoral radiomic features in differentiating the invasiveness of adenocarcinoma manifesting as ground-glass nodules. Eur Radiol 2021;31:9030-7.
25. Weng Q, Zhou L, Wang H, et al. A radiomics model for determining the invasiveness of solitary pulmonary nodules that manifest as part-solid nodules. Clin Radiol 2019;74:933-43.

Cite this article as: Wang Y, Lyu D, Yu D, Hu S, Ma Y, Huang W, Duan S, Zhou T, Tu W, Zhou X, Xiao Y, Fan L, Liu S. Intratumoral and peritumoral radiomics combined with computed tomography features for predicting the invasiveness of lung adenocarcinoma presenting as a subpleural ground-glass nodule with a consolidation-to-tumor ratio ≤50%. J Thorac Dis 2024;16(8):5122-5137. doi: 10.21037/jtd-24-243